Journal of Structural Biology 186 (2014) 431–437

Contents lists available at ScienceDirect

Journal of Structural Biology

journal homepage: www.elsevier.com/locate/yjsbi

Influence of repeat numbers on self-assembly rates of repetitive recombinant spider silk proteins

Martin Humenik, Michael Magdeburg, Thomas Scheibel *

Lehrstuhl Biomaterialien, Fakultät für Ingenieurwissenschaften, Universität Bayreuth, Universitätsstraße 30, 95440 Bayreuth, Germany

ARTICLE INFO

Article history:
Received 17 January 2014
Received in revised form 11 March 2014
Accepted 12 March 2014
Available online 20 March 2014

Keywords:
Self-assembly
Cross-β fibril
Kinetics
Polyalanine
Spider silk
Structure

ABSTRACT

Assembly of recombinant spider silk variants eADF4(C*n*) comprising different numbers (*n*) of the consensus sequence motif C, derived from the natural *Araneus diadematus* dragline silk ADF4, yielded indistinguishable nanofibrils in cases of $n \geqslant 2$. The C-module comprises 35 amino acids rich in glycine and proline residues (in GPGXY repeats) and one polyalanine stretch $(Ala)_8$. All variants were found to be intrinsically disordered in solution, and upon fibril formation they converted into a cross-β structure. Heterologous seeding indicated high structural compatibility between the different eADF4(C*n*) variants, however, their assembly kinetics differed in dependence of the number of repeats. Kinetic analysis revealed a nucleation-growth mechanism typical for the formation of cross-β-fibrils, with nucleation rates as well as growth rates increasing with increasing numbers of repeats. Strikingly, the single C-module did not self-assemble into fibrils, but upon addition of heterologous seeds fibril growth could be observed. Apparently, interconnecting of at least two C-modules significantly facilitates the structural transformation from a disordered state into β-sheet structures, which is necessary for nucleation and beneficial for fibril growth.

1. Introduction

Spider silk represents a fascinating material being mechanically strong and, at the same time, biocompatible (Humenik et al., 2011). One of the best understood spider silks, the so-called dragline of orb weaving spiders, exceeds any natural or artificial fiber in toughness (Gosline et al., 1999). Natural spider silks are, however, limited in availability based on both the cannibalistic behavior of spiders hampering farming and a complicated "silking" process to retrieve fibers. To circumvent the limitations in availability, different strategies have been established for biotechnological production of spider silk proteins (Heidebrecht and Scheibel, 2013; Tokareva et al., 2013). Recombinant spider silk proteins enabled development of silk materials like fibers (Xia et al., 2010), particles (Blüm and Scheibel, 2012; Numata et al., 2011), capsules (Blüm et al., 2014; Rabotyagova et al., 2010) and nanofibrils (Humenik and Scheibel, 2014; Numata and Kaplan, 2011; Rammensee et al., 2006; Slotta et al., 2007).

Spider silk proteins (spidroins) typically have high molecular weights (250–350 kDa), with primary sequences dominated by a repetitive core (>1000 amino acids) flanked by small globular amino- and carboxyterminal domains (100–150 amino acids) (Fig. 1). Consensus motifs of the dragline core repeats are composed of polyalanine stretches $(Ala)_n$ ($n = 4–12$) flanked by GA, GGX and GPGXY sequences (Rising et al., 2005). Interplay between the terminal domains and folding of the core domain results in hierarchical fiber assembling during an explicit spinning process (Eisoldt et al., 2011), including ionic exchange of chaotropic Na^+ and Cl^- against kosmotropic K^+ and PO_4^{3-}, a concomitant pH drop and water removal (Vollrath and Knight, 2001). In combination with shear forces, the spinning conditions result in the formation of antiparallel inter- and intrachain β-sheets being preferentially aligned in parallel to the fiber axis (Papadopoulos et al., 2009; van Beek et al., 2002).

Since the core domain of spider silk proteins lacks a defined tertiary structure in solution (Lefevre et al., 2011) they can be referred to as intrinsically disordered proteins (IDPs) (Uversky and Dunker, 2010). Intrinsic disorder of entire or partial protein sequences has been recognized as an important functional feature for many eukaryotic proteins (Chouard, 2011). Additionally, IDPs are better suited to convert their soluble structure into one of insoluble cross-β fibrils (Jahn et al., 2010) in comparison to tightly folded

* Corresponding author. Address: Bayreuther Zentrum für Kolloide und Grenzflächen (BZKG), Institut für Bio-Makromoleküle (bio-mac), Bayreuther Zentrum für Molekulare Biowissenschaften (BZMB), Bayreuther Materialzentrum (BayMAT), Universität Bayreuth, Universitätsstraße 30, 95440 Bayreuth, Germany.
E-mail address: thomas.scheibel@bm.uni-bayreuth.de (T. Scheibel).
URL: http://www.fiberlab.de (T. Scheibel).

http://dx.doi.org/10.1016/j.jsb.2014.03.010
1047-8477/

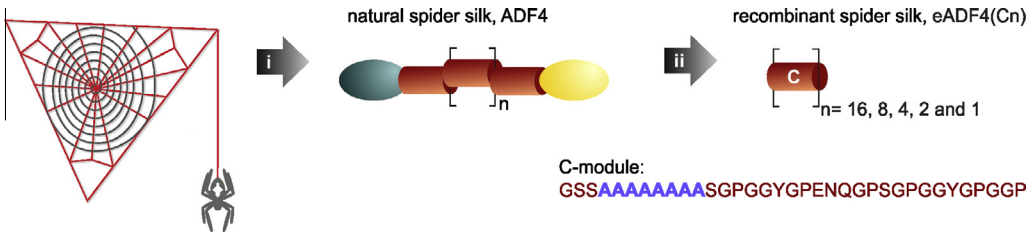

Fig.1. Composition of natural and recombinant spider silk proteins; (i) Dragline silk of the European garden spider (*A. diadematus)* comprises at least two major components ADF3 and ADF4, both showing a repetitive core domain (red) and small non-repetitive termini (green and yellow). (ii) The repeated consensus motif of the core domain of ADF4 (C-module) has been optimized for the production in *E. coli* (Huemmerich et al., 2004), and variants with different numbers of C-modules, eADF4(C*n*), were generated.

globular proteins due to higher conformational flexibility (Uversky, 2013).

The engineered spider silk protein eADF4(C16), comprising 16 times the consensus motif (C-module) of the core domain of dragline protein *Araneus diadematus* fibroin 4 (ADF4), self-assembles from disordered structure in solution into β-sheet rich nanofibrils exhibiting X-ray diffraction patterns typical for cross-β structures (Slotta et al., 2007). This self-assembly is triggered by cosmotropic phosphate ions similar to that of native spider silk. The C-module comprises 35 amino acids (Fig. 1) with one $(Ala)_8$ stretch forming β-sheets as well as glycine/proline rich GPGXY repeats remaining unstructured or helical upon assembly (Lefevre et al., 2011; Spiess et al., 2010).

Here, variants eADF4(C*n*) (Fig. 1) differing in number (*n* = 1, 2, 4, 8 and 16) of C-modules were analyzed concerning their assembly kinetics in order to determine the critical number of repeats required for nucleation and elongation of nanofibrils.

2. Material and methods

All chemicals used in this study had analytical grade purity. Sinapinic acid for MALDI TOF was obtained from Aldrich (Taufkirchen, Germany). All other chemicals were acquired form Carl Roth GmbH & Co. KG (Karlsruhe, Germany). Double-distilled water was prepared using a Millipore system (Merck Millipore, Merck KGaA, Darmstadt, Germany).

2.1. Protein production and purification

Proteins eADF4(C8) and eADF4(C16) were produced and purified as described previously (Huemmerich et al., 2004).

Variants eADF4(C4), (C2) and (C1) were produced and purified in fusion with a His_6-SUMO tag (Suhre and Scheibel, 2014). The cloning vectors pCS eADF4(C4), (C2) and (C1) were digested using BamHI and HindIII (New England BioLabs (NEB)) and designated inserts were ligated with a correspondingly digested pET28a(+)-vector (Novagen) encoding the His_6-SUMO tag using T4 Ligase (NEB). Constructs pET His_6-SUMO-eADF4(C*n*), *n* = 1, 2 and 4, were transformed into *E. coli* BL21(DE3)-GOLD (Novagen). The respective *E. coli* strain was fermented in LB Medium containing 35 μg/ml kanamycin and 0.001% (v/v) Breox FMT 30 antifoam (Cognis) using a 1.3 L Minifors reactor (Infors HT, Bottmingen, Switzerland). Gene expression was induced at an optical density OD_{600} = 45 using 1 mM IPTG, and fermentation continued at 30 °C for 4 h.

Cells pellets (100 g) were disrupted using a high pressure homogenisator Microfluidizer M110S (Microfluidics, USA-Newton), and 12.5 mg Protease-Inhibitor Mix-HP (SERVA, Heidelberg, Germany) was added to the suspension. Column chromatography was performed using an Äkta Purifier (GE Healthcare, Germany). After centrifugation, the supernatant was incubated with 20 mM imidazole and loaded onto a Ni–NTA chelating Sepharose column (50 mL, GE Healthcare) followed by washing with 50 mM Tris/HCl, 100 mM NaCl, 10 mM imidazole, pH 8 (buffer A) using three column volumes. The His_6-SUMO fusion proteins were eluted using 60% buffer B (50 mM Tris/HCl, 100 mM NaCl, 500 mM imidazole). The eluate was diluted six times using ddH_2O and the dilutant was loaded onto a Q-Sepharose column (150 mL, GE Healthcare), washed with 25 mM HEPES-Na, pH 8, and eluted using a gradient of 0–100% buffer B (25 mM HEPES-Na, 1 M NaCl) over five column volumes. Fusion proteins typically eluted at 150 mM NaCl, whereas remnants of bacterial DNA eluted at 700 mM NaCl. Pooled fractions were incubated subsequently with recombinant His_6-tagged *Saccharomyces cerevisiae* Ulp1 protease (1/1000 w/w) at 4 °C for 10 h. His_6-SUMO free eADF4(C*n*) was loaded onto a Ni–NTA column and collected in the flow through. eADF4(C*n*) was intensively dialyzed against 25 mM NH_4HCO_3 and lyophilized. The identity of the respective protein was confirmed by MALDI-TOF mass spectrometry analysis (Fig. S1; Table S1).

2.2. Protein characterization

2.2.1. FT-IR and CD spectroscopy

Soluble and assembled silk proteins were used at 1 mg/mL for FT-IR and at 0.2 mg/mL for CD-spectroscopy. FT-IR absorption spectra were recorded upon accumulation of 128 scans from 900 to 4000 cm^{-1} on a Bruker Tensor 27 (Bruker, Germany) spectrometer equipped with an AquaSpec™ Flow Cell (micro-biolytics GmbH, Germany), and spectral transformations were performed using OPUS software (version 6.5, Bruker Optik, GmbH). CD spectra were recorded upon accumulating five scans using a J-815 CD spectrometer (Jasco, Germany).

2.2.2. MALDI-TOF mass spectrometry

MALDI-TOF mass spectrometry was performed on a Bruker Reflex III (Bruker, Germany) equipped with a 337 nm N_2 laser in a linear mode and 20 kV acceleration voltages. Data were processed using mMass 5.1.0 software (Strohalm et al., 2008). Proteins, dialyzed in 25 mM NH_4HCO_3, were mixed in 1/1 ratio with a matrix solution (20 mg/ml sinapinic acid in 90% acetonitrile and 0.2% trifluoroacetic acid) before spotting onto a target plate.

2.3. Characterization of fibrils

eADF4(C*n*) was typically dissolved in 6 M GdmSCN, extensively dialyzed against 10 mM Tris/HCl, pH 8, and then centrifuged in a Beckman Optima ultracentrifuge at 185,000*g* for 1 h at 4 °C. Fresh protein solutions were prepared to exclude presence of oligomers before assembly. Protein self-assembly was initiated by addition of 100–200 mM potassium phosphate buffer (KPi), pH 8.

2.3.1. Congo Red binding experiments

Congo Red (CR) (5 μM) was mixed either with soluble or assembled proteins at 0.5 mg/mL in 10 mM Tris/HCl. Baselines of fibril suspensions were recorded at the same protein concentration, to

correct the CR spectra for light scattering. UV–VIS spectrometry was performed using a Cary 50 Bio spectrometer (Varian, Germany).

2.3.2. Thioflavin T binding experiments

Soluble and assembled proteins were diluted to 0.25 mg/mL using 10 mM Tris/HCl, pH 8, and incubated with 3 μM Thioflavin T (ThT) for 10 min. Fluorescence spectra were recorded using a FP-6500 fluorescence spectrometer at an excitation wavelength of 450 nm (Jasco, Germany).

2.3.3. AFM and TEM imaging

Assembled fibrils were diluted to 0.5 mg/ml. For AFM analysis, 40 μL of the fibril dilution were spotted on freshly-cleaved mica plates (Ø 10 mm, V1 grade, Plano GmbH, Germany), incubated for 5 min and subsequently washed four times using 50 μL of ddH_2O. For TEM analysis, 2 μL of the fibril dilution were spotted on supports (Pioloform-carbon-coated 200-mesh copper grids (Plano GmBH, Germany)), incubated for 2 min, washed four times using 5 μL of ddH_2O, and fibrils were negatively stained using 5 μL of 2% uranyl acetate solution. AFM and TEM samples were allowed to dry for 16 h at ambient temperature before imaging.

AFM scanning of dried samples was performed using a Dimension™ 3100 device equipped with a NanoScope® V controller (Veeco Instruments Inc., USA) using Si_3N_4 cantilevers (OMCL-AC160TS, Olympus, spring constant of 42 N/m, resonance frequency of 300 kHz, tip radius less than 7 nm) and operating in TappingMode™. AFM scans were processed using NanoScope Analysis software Version 1.40r3 (Brucker, Santa Barbara, CA).

TEM imaging of dry samples was performed with a JEM-2100 transmission electron microscope (JEOL, Tokyo, Japan) operated at 80 kV. Images were recorded using a 4000 × 4000 charge-coupled device camera (UltraScan 4000; Gatan, Pleasanton, CA) and Gatan Digital Micrograph software (version 1.70.16.).

2.4. Analysis of assembly kinetics using turbidity measurements and ultracentrifugation

Proteins were dissolved in 6 M GdmSCN, dialyzed extensively against 10 mM Tris/HCl, pH 8 and ultracentrifuged at 185,000g at 4 °C for 1 h. Samples (140 μL) were prepared in triplicate at distinct protein concentrations, and assembly was started upon addition of KPi buffer, pH 8. For turbidity measurements, absorption at 340 nm was recorded every 10–30 min during the aggregation course. Additionally, samples were centrifuged at specified time points at 185,000g at 4 °C for 30 min, and the concentration of monomeric species in the supernatant was determined by UV spectroscopy at 280 nm.

To prepare seeds, suspensions of mature fibrils (200 μL, 2 mg/ml) were treated with a MS73 sonication probe (Bandelin, Germany) at 10% amplitude for 15 s. This cycle was repeated six times while keeping the samples on ice.

2.5. Kinetic models

2.5.1. Finke–Watzky two-step model

$$B_t = A_0 - \frac{\frac{k_1}{k_2} - A_0}{1 + \frac{k_1}{k_2 A_0} e^{(k_1 + k_2 A_0)t}} \quad (1)$$

B_t represents aggregated protein, A_0 the initial monomer concentration, k_1 the rate constant of nucleation and k_2 the rate constant of fibril growth by monomer addition. This model has been shown to fit assembly kinetics of several fibrous proteins (Morris et al., 2008). It describes fibril formation in two steps; A → B and A + B → 2B, with A representing the precatalytic protein form and B the converted catalytic form. The first reaction represents nucleation, whereas the second autocatalytic reaction represents fibril growth (Morris et al., 2009).

2.5.2. Logistic function

$$Y = y_i - m_i x + \frac{y_f - m_f x}{1 + e^{-[(x - x_0)/\tau]}} \quad (2)$$

$$\text{Lag time} = x_0 - 2\tau \quad (3)$$

$y_i - m_i x$ is the initial slope during the lag phase and $y_f - m_f x$ the initial slope after the growth phase; x_0 is the time at 50% conversion. The apparent rate constant k_{app} is given by $1/\tau$, and the lag phase is calculated by Eq. (3). This method enables convenient comparison of different fibril assembly kinetics, but it cannot mechanistically describe molecular events (Morris et al., 2008; Nielsen et al., 2001).

2.5.3. Pseudo first order kinetics

For seeded assembly it has been previously assumed that the number of active ends remains constant during the reaction course. (Naiki et al., 1997; O'Nuallain et al., 2004). Thus, the equation Monomer (M) + Seed (S) <=> Seed (S) represents a pseudo first order reaction described by

$$M_L = M_0 \cdot e^{-k_2 t}, \quad (4)$$

whit M_L representing monomers in solution and M_0 the total monomer concentration. The concentration of fibril bound monomers is given by

$$M_F = M_0 - M_L, \quad (5)$$

thus the change in its concentration can be described as

$$M_F = M_0 - M_0 e^{-k_2} \quad (6)$$

Since the turbidity signal y is directly proportional to the assembled protein fraction

$$Y = b \cdot M_F \quad (7)$$

(see Section 3.2 and Fig. S4), seeded assembly can be described with

$$y = y_0 - y_0 \cdot e^{-k_2 \cdot t} \quad (8)$$

3. Result and discussion

3.1. Assembly of spider silk variants comprising different numbers of repeats

Assembly of the recombinant spider silk protein eADF4(C16) could be triggered upon addition of kosmotropic phosphate ions (Pi). Nanofibrils assembled in aqueous buffers containing < 300 mM Pi, whereas above this threshold concentration particles were formed (Slotta et al., 2008).

Similarly to eADF4(C16), eADF4(C*n*) variants comprising 2–8 C modules were able to self-assemble into nanofibrils in presence of 100–200 mM potassium phosphate (KPi), pH 8. Transmission electron microscopy (TEM) revealed nanofibril diameters around 10 nm (Fig. 2A–D). Cross sectional analysis of atomic force microscopy (AFM) scans (Fig. 2E–H) showed heights in the range of 2–3 nm. The gained nanofibrils were indistinguishable to eADF4(C16) fibrils assembled under similar conditions. Strikingly, eADF4(C1) did not self-assemble under these conditions. No fibrils or aggregates were observed using TEM or AFM and no protein

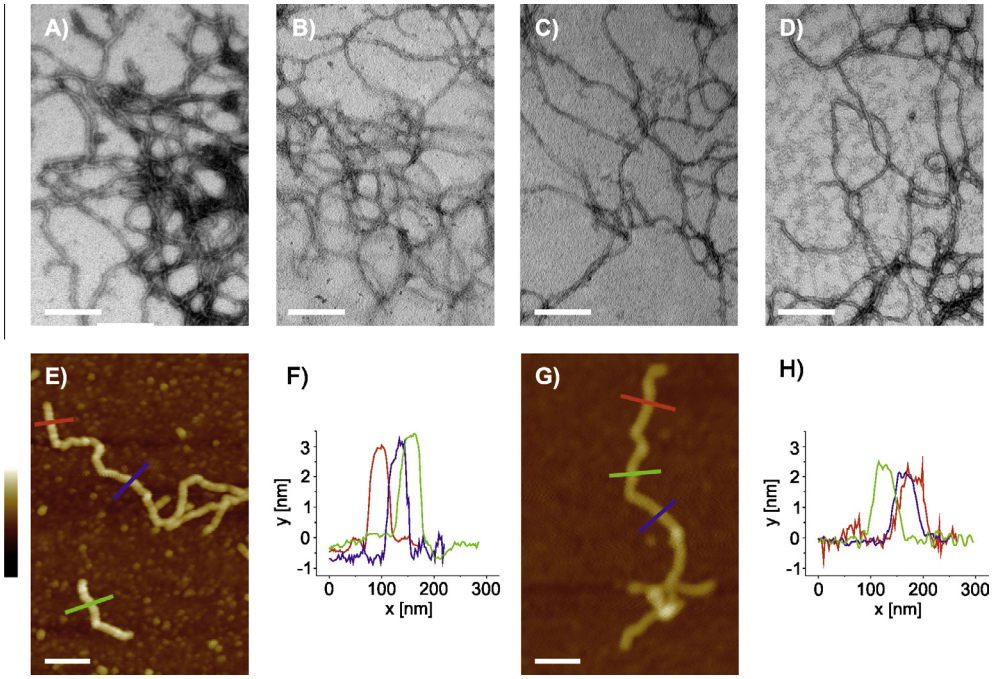

Fig.2. Morphology of self-assembled recombinant spider silk variant fibrils. (A–D) TEM images of eADF4(C16), (C8), (C4) and (C2) fibrils, respectively. (E, G) AFM scans of eADF4(C16) and (C4) fibrils, respectively. Height profiles in (F) and (H) correspond to the cross sectional analysis in (E) and (G) as indicated by blue, green and red lines, respectively. Scale bars represent 100 nm for the upper and 200 nm for the lower panel. The color bar on the left side of the lower panel represents heights from −5 nm (dark brown) to 5 nm (white).

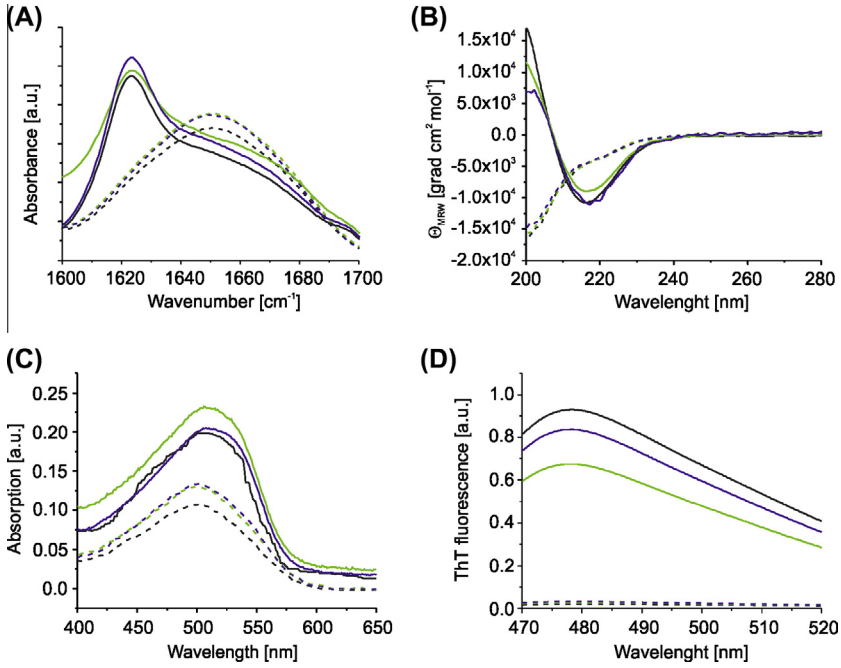

Fig.3. Structural characterization of fibrils prepared from different recombinant spider silk variants. FT-IR (A) and CD spectra (B) of the soluble variants (dashed lines) eADF4(C2) (grey), eADF4(C4) (green) and eADF4(C8) (blue) and the insoluble fibrils (solid lines) thereof. Congo Red (C) and Thioflavin T (D) spectra of the identical samples.

structural changes could be detected using CD spectrometry (Fig. S2).

Next, we analyzed secondary structures of the variants by FT-IR spectroscopy, especially focusing on characteristic peptide bond vibrations represented by Amide I bands (1600–1700 cm^{-1}, C=O stretching) (Hu et al., 2006; Krishnaji et al., 2013; Rabotyagova et al., 2010; Spiess et al., 2010, 2011). All soluble silk variants revealed FT–IR pattern typical for IDPs. The Amide I band maximum at 1650 cm^{-1} (Fig. 3A) is indicative for helical/random coil conformations (Humenik and Scheibel, 2014; Slotta et al., 2006; Spiess et al., 2010). This structure was further confirmed by CD-spectra with local minimum at 200 nm (Fig. 3B), indicative of unstructured proteins (Kelly et al., 2005; Uversky, 2002) comprising polyproline II (PPII) conformations (Chen et al., 2004; Ding

et al., 2003; Shi et al., 2005). The fibrils were, however, rich in β-sheets as demonstrated by FT–IR spectra with a shifted Amide I band towards 1624 cm^{-1} (Fig. 3A) and minima at 218 nm in the CD spectra (Goldsbury et al., 2000a; Kelly et al., 2005) (Fig. 3B). eADF4(C16) nanofibrils showed cross-β sheet structures as determined by CR and ThT binding (Slotta et al., 2007), since these molecular probes commonly bind to cross-β structure of protein fibrils (Groenning, 2010). Here, incubation of eADF4(C*n*) variant fibrils with CR resulted in a red shift of λ_{max} from 500 to 514 nm (Fig. 3C), and incubation with ThT (Fig. 3D) yielded an increase in the dye fluorescence maximum at 476 nm.

3.2. Assembly kinetics of spider silk variants

Since morphology and structure of eADF4(C*n*) fibrils was independent of the number of repeats (between 2 and 16), we next studied assembly kinetics of the variants. Turbidity measurements were employed at 340 nm. Although the method is generally not suitable for comparison of different proteins due to a strong signal dependency on aggregate size (Andreu and Timasheff, 1986; Goldsbury et al., 2000b), the observed morphological similarities, *i.e.*, length and diameter of the eADF4(C*n*) fibrils (Fig. 2) allowed turbidity measurements (similar final plateaus at 1.1–1.4 a.u., Figure S3A–D) to get insights into assembly kinetics of the variants. Since the final plateaus reflected a complete depletion of soluble monomers, it was assumed, that the normalized turbidity signals correlate with the fraction of assembled protein as confirmed by ultracentrifugation of fibrils at different assembly time points (compare Fig. S4 and Fig. 4A).

The variants' self-assembly revealed kinetics of sigmoidal shapes (Fig. 4A). Initial lag phases corresponded to formation of thermodynamically disfavored oligomeric species being in equilibrium with soluble monomers. Once oligomers reached a distinct structure and a critical size, they acted as nuclei for monomer addition resulting in exponential fibril growth (Cohen et al., 2012; Morris et al., 2009). Data points could be fitted (R^2 = 0.995–0.999; Table 1) using the Finke–Watzky (F–W) two-step model (Eq. 1). Interestingly, silk variants showed decreasing lag times (Table S2) and exponentially increasing growth rates (k_2) (Fig. S3G) with increasing numbers of repetitive units. Therefore, the repetitive arrangement of C-modules was required for the conversion of intrinsically disordered monomeric eADF4(C*n*) towards an oligomeric β-sheet structure. This finding was supported by the observation that eADF4(C1) did not self-assemble (Fig. 4A). Upon structural conversion, hydrogen bonds of disordered polypeptide chains have to be broken before new interstrand hydrogen bonds of β-sheets can be formed. In case of eADF4(C*n*), repetitive interconnection of polylalanine stretches might play an important role. Previously, molecular simulations have shown that interaction of two β-stands in an antiparallel manner is ineffective if no linkage is present (Ma and Nussinov, 2000), thus explaining the observed differences in self-assembly between eADF4(C1) and eADF4(C2)–(C16).

3.3. Seeded assembly kinetics of spider silk variants

Homologous and heterologous seeded assembly of eADF4(Cn) variants was determined by turbidity measurements, and obtained data were fitted to pseudo first order kinetics introduced by Naiki et al., (Eq. (7)). Seeds were prepared by sonication of mature fibrils resulting in significantly shortened fibrils, thus, multiplying active fibrils ends (O'Nuallain et al., 2004). Addition of homologous seeds to soluble monomers readily eliminated the lag phase (exemplarily shown in Fig. S5) confirming the nucleation mechanism of eADF4(Cn) assembly. The seeds effectively by-passed the thermodynamically disfavored oligomerisation within the lag phase (Fig. 4A). Heterologous "cross" seeding using eADF4(C16) seeds to initiate eADF4(Cn) assembly (Fig. 4B) was employed to address the structural similarity of the nucleating interface (Jayaraman et al., 2009; O'Nuallain et al., 2004). Heterologous seeds were able

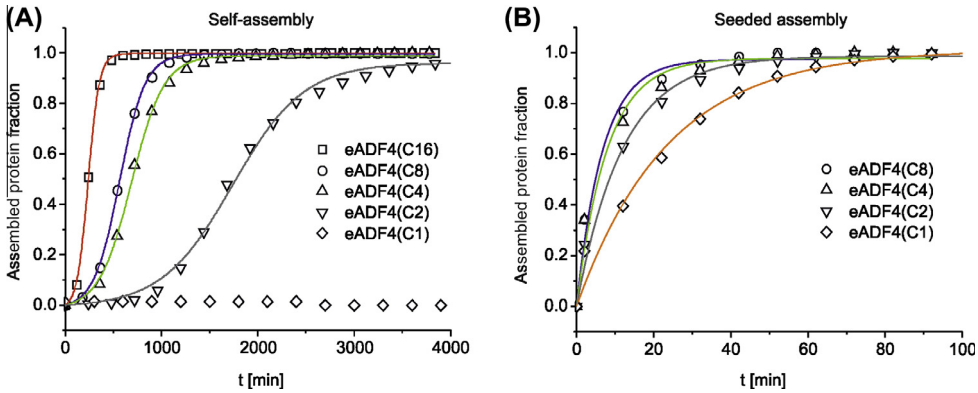

Fig.4. Assembly kinetics of recombinant spider silk variants. (A) Assembly of eADF4(C*n*) at 2 mg/mL upon addition of 150 mM KPi. Data points were fitted using the F–W two step model (Eq. (1)). (B) Assembly started upon addition of eADF4(C16) seeds (5% w/w). Data points were fitted to a pseudo-first order kinetic (Eq. (7)) (Naiki et al., 1997).

Table 1
Kinetic parameters of unseeded and seeded assembly of spider silk variants. Assembly kinetics were performed at 2 mg/mL. The molar C-module concentration of all variants was identical (631 μM).

	eADF4(C16) (41.9 μM)	eADF4(C8) (81.6 μM)	eADF4(C4) (169.3 μM)	eADF4(C2) (330.3 μM)	eADF4(C1) (631.0 μM)
F–W model for nucleated assembly					
k_1 (min^{-1})	2.63E–04	1.04E–04	9.66E–05	2.41E–05	n.d.
k_2 ($\mu M^{-1}.min^{-1}$)	4.11E–04	9.15E–05	3.50E–05	8.47E–06	n.d.
R^2	0.999	0.999	0.998	0.995	n.d.
Pseudo first order kinetic for seeded assembly					
seeded k_{2app} (min^{-1})	0.151	0.147	0.126	0.083	0.042
R^2	0.979	0.986	0.978	0.991	0.985

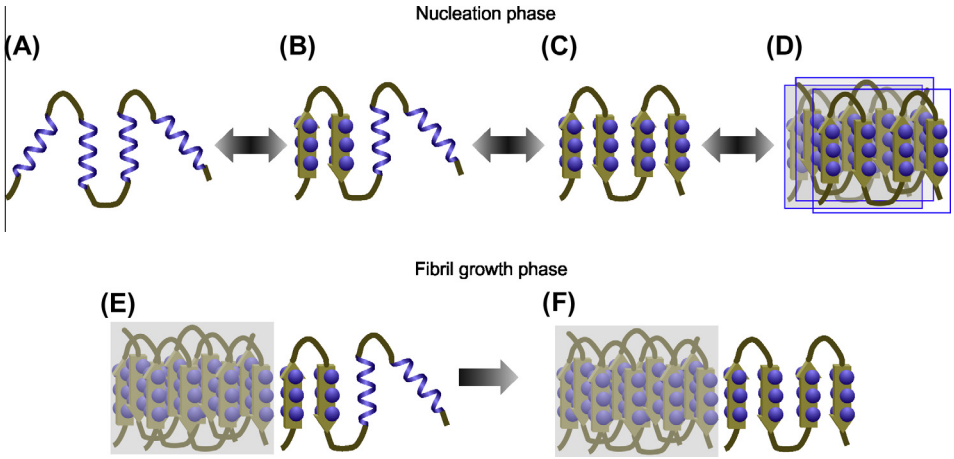

Fig.5. Model of cross-β fibril assembly of eADF4(C*n*). eADF4(C4) is shown exemplarily. (A) Intrinsically disordered eADF4(C4) monomer; (B, C) Structural transformation towards antiparallel β-sheets; (D) Formation of a nucleus via hydrophobic interactions of polyalanine β-sheets (simplified here as blue spheres; layer borders are highlighted as pale blue squares); (E) Docking of further monomers onto the nucleus/fibril end; (F) Facilitated fibril elongation.

to eliminate the lag phase (compare Fig. 4A and B) similarly to homologous seeds (Fig. S5). Pseudo first order rate constants of seeded reactions were 10 times higher than the apparent rate constants of respective unseeded self-assembly (Tables 1 and S2) at the same monomer concentration. Interestingly, eADF4(C2) seeds were apparently more efficient in initiating eADF4(C16) assembly than homologous eADF4(C16) seeds (Fig. S5A, compare squares and circles). The heterologous seeding experiments implied that fibrils made of the different spider silk variants are structurally highly compatible as already indicated by TEM, AFM, FT-IR and CD spectroscopy (Figs. 2 and 3). Surprisingly, eADF4(C1) seeded with eADF4(C16) seeds yielded also nanofibrils (compare Fig. 4A and B), indicating that although the single C-module is unable to form a nucleus (Fig. 4A) it can be added onto free fibril ends/seeds probably due to a templating mechanism (Esler et al., 2000; Pellarin et al., 2007; Straub and Thirumalai, 2011).

4. Conclusion

Based on the structural and kinetic data, eADF4(C*n*) assembly into cross β-sheet fibrils can be described by two phases (Fig. 5). In the nucleation phase intrinsically disordered silk monomers with distinct local structures (e.g. polylalanine PPII helices) (Fig. 5A) transiently convert into antiparallel β-sheets in a process being facilitated by interlinked polyalanine stretches in neighboring C-modules (Fig. 5B). The structures are stabilized by hydrogen bonding of $(Ala)_8$ β-sheets (Fig. 5C). Such cooperative folding is impossible for eADF4(C1) possessing only one polyalanine stretch. Folded eADF4(Cn) proteins form a nucleus (Fig. 5D), which is stabilized *via* hydrophobic interactions of exposed Ala residues (Nguyen and Hall, 2004). In the elongation phase monomer addition occurs *via* so-called dock-lock mechanism (Straub and Thirumalai, 2011). Docking of the monomer to the exposed fibril ends (Fig. 5E) is followed by a structural transformation of the monomer gaining a new nucleation interface (Fig. 5F). Apparently, the formation of local antiparallel β-sheets was accelerated in variants containing higher numbers of repeats, which resulted in faster nucleation and faster fibril growth.

Acknowledgments

This work was supported by the Deutsche Forschungsgemeinschaft (DFG Grant No. SCH 603/9-1). We thank A. Pfaffenberger for MALDI-TOF measurements and K. Schacht for TEM imaging.

Appendix A. Supplementary data

Supplementary data associated with this article can be found, in the online version, at http://dx.doi.org/10.1016/j.jsb.2014.03.010.

References

Andreu, J.M., Timasheff, S.N., 1986. The measurement of cooperative protein self-assembly by turbidity and other techniques. In: Hirs, C.H.W., Timasheff, S.N. (Eds.), Methods Enzymology, vol. 130. Academic Press, pp. 47–59.
Blüm, C., Scheibel, T., 2012. Control of drug loading and release properties of spider silk sub-microparticles. BioNanoScience 2, 67–74.
Blüm, C., Nichtl, A., Scheibel, T., 2014. Spider silk capsules as protective reaction containers for enzymes. Adv. Funct. Mater. 24, 763–768.
Chen, K., Liu, Z., Kallenbach, N.R., 2004. The polyproline II conformation in short alanine peptides is noncooperative. Proc. Natl. Acad. Sci. U.S.A. 101, 15352–15357.
Chouard, T., 2011. Structural biology: breaking the protein rules. Nature 471, 151–153.
Cohen, S.I.A., Vendruscolo, M., Dobson, C.M., Knowles, T.P.J., 2012. From macroscopic measurements to microscopic mechanisms of protein aggregation. J. Mol. Biol. 421, 160–171.
Ding, L., Chen, K., Santini, P.A., Shi, Z., Kallenbach, N.R., 2003. The pentapeptide GGAGG has PII conformation. J. Am. Chem. Soc. 125, 8092–8093.
Eisoldt, L., Smith, A., Scheibel, T., 2011. Decoding the secrets of spider silk. Mater. Today 14, 80–86.
Esler, W.P., Stimson, E.R., Jennings, J.M., Vinters, H.V., Ghilardi, J.R., Lee, J.P., Mantyh, P.W., Maggio, J.E., 2000. Alzheimer's disease amyloid propagation by a template-dependent dock-lock mechanism. Biochemistry 39, 6288–6295.
Goldsbury, C., Goldie, K., Pellaud, J., Seelig, J., Frey, P., Müller, S.A., Kistler, J., Cooper, G.J.S., Aebi, U., 2000a. Amyloid fibril formation from full-length and fragments of amylin. J. Struct. Biol. 130, 352–362.
Goldsbury, C.S., Wirtz, S., Müller, S.A., Sunderji, S., Wicki, P., Aebi, U., Frey, P., 2000b. Studies on the in vitro assembly of Aβ 1–40: Implications for the search for Aβ fibril formation inhibitors. J. Struct. Biol. 130, 217–231.
Gosline, J.M., Guerette, P.A., Ortlepp, C.S., Savage, K.N., 1999. The mechanical design of spider silks: from fibroin sequence to mechanical function. J. Exp. Biol. 202, 3295–3303.
Groenning, M., 2010. Binding mode of thioflavin T and other molecular probes in the context of amyloid fibrils—current status. J. Chem. Biol. 3, 1–18.
Heidebrecht, A., Scheibel, T., 2013. Recombinant production of spider silk proteins. Adv. Appl. Microbiol. 82, 115–153.
Hu, X., Kaplan, D., Cebe, P., 2006. Determining beta-sheet crystallinity in fibrous proteins by thermal analysis and infrared- spectroscopy. Macromolecules 39, 6161–6170.
Huemmerich, D., Helsen, C.W., Quedzuweit, S., Oschmann, J., Rudolph, R., Scheibel, T., 2004. Primary structure elements of spider dragline silks and their contribution to protein solubility. Biochemistry 43, 13604–13612.
Humenik, M., Scheibel, T., 2014. Nanomaterial building blocks based on spider silk–oligonucleotide conjugates. ACS Nano 8, 1342–1349.
Humenik, M., Scheibel, T., Smith, A., 2011. Spider silk: Understanding the structure–function relationship of a natural fiber. In: Stefan, H. (Ed.), Progress in Molecular Biology and Translational Science. Academic Press, pp. 131–185.
Jahn, T.R., Makin, O.S., Morris, K.L., Marshall, K.E., Tian, P., Sikorski, P., Serpell, L.C., 2010. The common architecture of cross-β amyloid. J. Mol. Biol. 395, 717–727.

Jayaraman, M., Kodali, R., Wetzel, R., 2009. The impact of ataxin-1-like histidine insertions on polyglutamine aggregation. Protein Eng. Des. Sel. 22, 469–478.
Kelly, S.M., Jess, T.J., Price, N.C., 2005. How to study proteins by circular dichroism. Biochim. Biophys. Acta, Proteins Proteomics 1751, 119–139.
Krishnaji, S.T., Bratzel, G., Kinahan, M.E., Kluge, J.A., Staii, C., Wong, J.Y., Buehler, M.J., Kaplan, D.L., 2013. Sequence–structure–property relationships of recombinant spider silk proteins: Integration of biopolymer design, processing, and modeling. Adv. Funct. Mater. 23, 241–253.
Lefevre, T., Boudreault, S., Cloutier, C., Pezolet, M., 2011. Diversity of molecular transformations involved in the formation of spider silks. J. Mol. Biol. 405, 238–253.
Ma, B., Nussinov, R., 2000. Molecular dynamics simulations of a β-hairpin fragment of protein G: balance between side-chain and backbone forces. J. Mol. Biol. 296, 1091–1104.
Morris, A.M., Watzky, M.A., Agar, J.N., Finke, R.G., 2008. Fitting neurological protein aggregation kinetic data via a 2-step, minimal/"Ockham's razor" model: the Finke–Watzky mechanism of nucleation followed by autocatalytic surface growth. Biochemistry 47, 2413–2427.
Morris, A.M., Watzky, M.A., Finke, R.G., 2009. Protein aggregation kinetics, mechanism, and curve-fitting: a review of the literature. Biochim. Biophys. Acta, Proteins Proteomics 1794, 375–397.
Naiki, H., Hashimoto, N., Suzuki, S., Kimura, H., Nakakuki, K., Gejyo, F., 1997. Establishment of a kinetic model of dialysis-related amyloid fibril extension in vitro. Amyloid 4, 223–232.
Nguyen, H.D., Hall, C.K., 2004. Molecular dynamics simulations of spontaneous fibril formation by random-coil peptides. Proc. Natl. Acad. Sci. U.S.A. 101, 16180–16185.
Nielsen, L., Khurana, R., Coats, A., Frokjaer, S., Brange, J., Vyas, S., Uversky, V.N., Fink, A.L., 2001. Effect of environmental factors on the kinetics of insulin fibril formation: elucidation of the molecular mechanism. Biochemistry 40, 6036–6046.
Numata, K., Kaplan, D.L., 2011. Differences in cytotoxicity of beta-sheet peptides originated from silk and amyloid beta. Macromol. Biosci. 11, 60–64.
Numata, K., Reagan, M.R., Goldstein, R.H., Rosenblatt, M., Kaplan, D.L., 2011. Spider silk-based gene carriers for tumor cell-specific delivery. Bioconjugate Chem. 22, 1605–1610.
O'Nuallain, B., Williams, A.D., Westermark, P., Wetzel, R., 2004. Seeding specificity in amyloid growth induced by heterologous fibrils. J. Biol. Chem. 279, 17490–17499.
Papadopoulos, P., Solter, J., Kremer, F., 2009. Hierarchies in the structural organization of spider silk-a quantitative model. Colloid Polym. Sci. 287, 231–236.
Pellarin, R., Guarnera, E., Caflisch, A., 2007. Pathways and intermediates of amyloid fibril formation. J. Mol. Biol. 374, 917–924.
Rabotyagova, O.S., Cebe, P., Kaplan, D.L., 2010. Role of polyalanine domains in beta-sheet formation in spider silk block copolymers. Macromol. Biosci. 10, 49–59.
Rammensee, S., Huemmerich, D., Hermanson, K.D., Scheibel, T., Bausch, A.R., 2006. Rheological characterization of hydrogels formed by recombinantly produced spider silk. Appl. Phys. A: Mater. Sci. Process. 82, 261–264.
Rising, A., Nimmervoll, H., Grip, S., Fernandez-Arias, A., Storckenfeldt, E., Knight, D.P., Vollrath, F., Engstrom, W., 2005. Spider silk proteins-mechanical property and gene sequence. Zool. Sci. 22, 273–281.
Shi, Z.S., Chen, K., Liu, Z.G., Ng, A., Bracken, W.C., Kallenbach, N.R., 2005. Polyproline II propensities from GGXGG peptides reveal an anticorrelation with beta-sheet scales. Proc. Natl. Acad. Sci. U.S.A. 102, 17964–17968.
Slotta, U., Tammer, M., Kremer, F., Koelsch, P., Scheibel, T., 2006. Structural analysis of spider silk films. Supramol. Chem. 18, 465–471.
Slotta, U., Hess, S., Spiess, K., Stromer, T., Serpell, L., Scheibel, T., 2007. Spider silk and amyloid fibrils: a structural comparison. Macromol. Biosci. 7, 183–188.
Slotta, U.K., Rammensee, S., Gorb, S., Scheibel, T., 2008. An engineered spider silk protein forms microspheres. Angew. Chem. Int. Ed. 47, 4592–4594.
Spiess, K., Wohlrab, S., Scheibel, T., 2010. Structural characterization and functionalization of engineered spider silk films. Soft Matter 6, 4168–4174.
Spiess, K., Ene, R., Keenan, C.D., Senker, J., Kremer, F., Scheibel, T., 2011. Impact of initial solvent on thermal stability and mechanical properties of recombinant spider silk films. J. Mater. Chem. 21, 13594–13604.
Straub, J.E., Thirumalai, D., 2011. Toward a molecular theory of early and late events in monomer to amyloid fibril formation. Annu. Rev. Phys. Chem. 62, 437–463.
Strohalm, M., Hassman, M., Košata, B., Kodíček, M., 2008. MMass data miner: an open source alternative for mass spectrometric data analysis. Rapid Commun. Mass Spectrom. 22, 905–908.
Suhre, M.H., Scheibel, T., 2014. Structural diversity of a collagen-binding matrix protein from the byssus of blue mussels upon refolding. J. Struct. Biol. 186, 75–85.
Tokareva, O., Michalczechen-Lacerda, V.A., Rech, E.L., Kaplan, D.L., 2013. Recombinant DNA production of spider silk proteins. Microb. Biotechnol. 6, 651–663.
Uversky, V.N., 2002. Natively unfolded proteins: a point where biology waits for physics. Protein Sci. 11, 739–756.
Uversky, V.N., 2013. Under-folded proteins: Conformational ensembles and their roles in protein folding, function, and pathogenesis. Biopolymers 99, 870–887.
Uversky, V.N., Dunker, A.K., 2010. Understanding protein non-folding. Biochim. Biophys. Acta, Proteins Proteomics 1804, 1231–1264.
van Beek, J.D., Hess, S., Vollrath, F., Meier, B.H., 2002. The molecular structure of spider dragline silk: folding and orientation of the protein backbone. Proc. Natl. Acad. Sci. U.S.A. 99, 10266–10271.
Vollrath, F., Knight, D.P., 2001. Liquid crystalline spinning of spider silk. Nature 410, 541–548.
Xia, X.X., Qian, Z.G., Ki, C.S., Park, Y.H., Kaplan, D.L., Lee, S.Y., 2010. Native-sized recombinant spider silk protein produced in metabolically engineered *Escherichia Coli* results in a strong fiber. Proc. Natl. Acad. Sci. U.S.A. 107, 14059–14063.